Available online at www.sciencedirect.com

ScienceDirect

Advances in Space Research xxx (xxxx) xxx

ADVANCES IN SPACE RESEARCH (a COSPAR publication)

www.elsevier.com/locate/asr

Use of GNSS and ERA5 precipitable water vapor based standardized precipitation conversion index for drought monitoring in the Mediterranean coast: A first case study in Southern Spain

Leire Retegui Schiettekatte [a,b,e], María Selmira Garrido [a,b,c], María Clara de Lacy [b,c,d,*]

[a] Department of Cartographic and Geodetic Engineering, Superior Polytechnic School, University of Jaén, Campus Las Lagunillas s/n 23071, Jaén, Spain
[b] Research group RNM282, University of Jaén, Campus Las Lagunillas s/n 23071, Jaén, Spain
[c] Center for Advanced Studies in Earth Sciences, Energy and Environment (CEACTEMA), University of Jaén, Campus Las Lagunillas s/n 23071, Jaén, Spain
[d] University San Pablo-CEU, CEU Universities, Department of Applied Mathematics and Data Science, Campus de Moncloa C/Julián Romea 23 28003, Madrid, Spain
[e] Geodesy Group, Department of Sustainability and Planning, Aalborg University, Rendsburggade 14 9000, Aalborg, Denmark

Received 12 January 2023; received in revised form 17 August 2023; accepted 18 August 2023

Abstract

In this paper the Standardized Precipitation Conversion Index (SPCI), a PWV-based drought index, has been computed using GNSS and ERA5 PWV and its performance has been tested with respect to the Standardized Precipitation Evapotranspiration Index (SPEI) in Southern Spain. One of the climatic features of this area is the low correlation level between PWV and precipitation, in contrast with other areas in which SPCI has been previously tested. The GNSS-SPCI has been derived from validated ZTD time series estimated from local GNSS permanent stations' data. All the needed meteorological values were derived from ERA5, excepting precipitation values and SPEI-SPI values which were extracted from a national high-resolution dataset.

The resulting SPCI time series have shown high correlation coefficients with respect to the SPEI. The use of longer SPCI time series allowed by ERA5 model has provided the most coherent results, suggesting that the ERA5-PWV data can be interesting to overcome problems caused by the short timespan of GNSS time series in SPCI computation. In general, high correlation coefficients have been obtained compared to global results from previous studies. This shows that, even for regions with low correlation levels between PWV and precipitation, the SPCI can have an interesting potential for drought monitoring. The SPCI was found to perform better on higher timescales (12 and 24 months). The performance of SPCI has also been compared that of the SPI: SPCI is able to outperform SPI for the 24-month timescale for a limited geographical region. This supports that the inclusion of PWV data in drought monitoring indices could be promising and is worth keeping to be investigated.

Keywords: PWV; SPCI; SPEI; SPI; ERA5; GNSS

* Corresponding author at: Department of Applied Mathematics and Data Science, University San Pablo-CEU, Campus de Moncloa C/Julián Romea 23 28003, Madrid, Spain.
E-mail addresses: clara.lacy@ceu.es, mclacy@ujaen.es (M. Clara de Lacy).

https://doi.org/10.1016/j.asr.2023.08.030
0273-1177/

Please cite this article as: L. Retegui Schiettekatte, M. Selmira Garrido and M. Clara de Lacy, Use of GNSS and ERA5 precipitable water vapor based standardized precipitation conversion index for drought monitoring in the Mediterranean coast: A first case study in Southern Spain, Advances in Space Research, https://doi.org/10.1016/j.asr.2023.08.030

Nomenclature

GNSS-PWV estimation related abbreviations

GNSS	Global Navigation Satellite System
PWV	Precipitable Water Vapor
ZHD	Zenith Hydrostatic Delay
ZTD	Zenith Total Delay
ZWD	Zenith Wet Delay

Drought index related abbreviations

PE	Precipitation Effectiveness
SPCI	Standardized Precipitation Conversion Index
SPEI	Standardized Precipitation Evapotranspiration Index
SPI	Standardized Precipitation Index

1. Introduction

GNSS (Global Navigation Satellite Systems) technologies have seen a great advance in the last decades. This advance has led to the development of new by-products that can be used for a wide variety of purposes. One of these important by-products are the tropospheric delays (Zenith Total Delay, ZTD) estimated from GNSS observations. The ZTD is strongly related to the atmospheric Precipitable Water Vapor (PWV) through temperature and pressure and hence can be used for meteorological and climatological studies. While the use of the GNSS-ZTD and GNSS-PWV has been usually oriented to applications such as the study of extreme precipitation events or its integration in Numerical Weather Prediction models, there is very little literature exploring the potential of this variable for drought monitoring (Bordi et al., 2016). In recent years, some studies have tried to define GNSS-PWV-based drought monitoring indices and compare their performance with some widely used indices such as the Standardized Precipitation Index (SPI) or the Standardized Precipitation Evapotranspiration Index (SPEI). Bordi et al. (2015, 2016) first considered a Precipitation Effectiveness (PE), based on GNSS-PWV and precipitation data, to monitor drought/wet episodes and found a good correlation between PE and SPI. Based on these results, Zhao et al. (2020) suggested a new multi-time scale Standardized Precipitation Conversion Index (SPCI) and performed a global correlation analysis between SPCI and SPEI indices, finding good correlations (over 0.96) at a 12-month timescale for most of the world regions.

The SPCI consists of an interesting option between the SPI and more complex indices such as the SPEI. Unlike the SPI, which is only based on precipitation data, the SPCI accounts for temperature through the PWV, as these variables are generally very strongly correlated (Zhao et al., 2020). Its calculation is kept simple as only precipitation and PWV are involved, and the latter can be accurately sensed in real-time by using GNSS technologies (Ma et al., 2021).

Some local studies have been carried out to test the capacity of GNSS-derived ZTD, PWV, and SPCI for drought monitoring. Jiang et al. (2017) and Wang et al. (2018) found that PWV trends can be used for severe flood and drought event monitoring at a regional scale in Yunnan (China) and Australia, respectively. Zhao et al. (2019) and Li et al. (2022) found that the Thornthwaite (TH) model, which is frequently used for Potential Evapotranspiration (PET) computation in the SPEI estimation, can be significantly improved by including a GNSS-ZTD (or PWV), temperature and pressure data combination, and Ma et al. (2021) verified that SPCI is able to outperform SPEI in the Yunnan region, using a Comprehensive Index (CI) of the China Meteorological Administration as a reference. Zhao et al. (2021) also suggested a new Standardized ENSO Monitoring Index based on GNSS-ZTD and temperature data and found good correlations with both Sea Surface Temperature and SPEI-12 in Taiwan.

These studies support the potential of the SPCI or GNSS-PWV-related indices for drought monitoring purposes. Nevertheless, all the regions considered in the previous case studies (Australia, China and Taiwan) are characterized by a positive and very high correlation between PWV and temperature as well as positive and very high correlations between PWV and precipitation, according to the global results obtained by Zhao et al. (2020). Considering this fact, the next question arises: Does GNSS-PWV have the same potential for drought monitoring in regions where these correlations are weaker or inverse? This is the case for a wide area around the Mediterranean Sea that displays negative correlation coefficients between PWV and precipitation, as shown in Zhao et al. (2020). The Mediterranean region has proven to be increasingly affected by droughts in recent decades (Sousa et al., 2011; Tramblay et al., 2013; Vicente-Serrano et al., 2014; Spinoni et al., 2015) and will be prone to severe drought events along with high socioeconomic implications under the climate change scenario (Gu et al., 2020). Therefore, it is very interesting to evaluate the capacity of SPCI for drought monitoring in these regions. This work constitutes a first assessment of the usefulness of SPCI in a Mediterranean region such as the Autonomous Community of Andalucía, Southern Spain.

This territory provides a very interesting scenario for the study of PWV and SPCI. The 87.599 km^2 area is characterized by a steep topography and the influence of two different seas (Atlantic Ocean and Mediterranean Sea), which results in a great climatological variability. For example, in terms of precipitation, some of the driest zones such as the southeastern shore (Almería province) accumulate less

Please cite this article as: L. Retegui Schiettekatte, M. Selmira Garrido and M. Clara de Lacy, Use of GNSS and ERA5 precipitable water vapor based standardized precipitation conversion index for drought monitoring in the Mediterranean coast: A first case study in Southern Spain, Advances in Space Research, https://doi.org/10.1016/j.asr.2023.08.030

than 200 mm of annual precipitation, while the wettest areas in the southern part of the territory (Cádiz) can reach more than 1300 mm of accumulated annual precipitation (REDIAM, 2014).

To account for this variability, in this study the area has been divided into three different regions attending geographical criteria. The basin of the main river, the Guadalquivir, and the Sierra Morena mountain range (region 1) are located at the northwestern side of the Baetic Mountains Ranges. The Baetic Mountain Ranges (main mountain range system) constitutes region 2. The territories located at the eastern side of the Mountain Ranges constitute region 3. The whole area is uniformly covered by a regional permanent GNSS network that includes some stations that have been operating since 2005 and is completed by the national GNSS network, as well as some IGS (International GNSS Service) stations and stations of the bordering provinces. The location of the stations used in this study and the geographical region they belong to are shown in Fig. 1.

Some previous works have addressed PWV in this region (Ortiz de Galisteo et al., 2014, 2011; Priego et al., 2016; Torres et al., 2010). However, there was no attempt so far to use all the available GNSS stations of the territory for long-term PWV computation, nor to test the capacity of this data for drought monitoring. The main objective of this study is to compute long time series (spanning 7 to 15 years between 2007 and 2022) of GNSS-PWV over the whole area and to test the capacity of GNSS-derived as well as ERA5-derived SPCI for drought monitoring in this region. The article is organized as follows. The data set used and the processing methods are explained in Section 2. The obtained results are presented and discussed in Section 3: this includes the ZTD time series validation, the PWV time series validation, the SPCI-SPEI correlations analysis, the comparison with respect to worldwide results and the comparison between the performance of SPI and SPCI. At last, the article is closed with the conclusions.

2. Data set and methods

2.1. GNSS data

GNSS permanent stations distributed over Southern Spain have been used for the GNSS-ZTD computation. These belong to four different networks: the regional network RAP (Andalusian Positioning Network, Red RAP | Portal Geodésico de Andalucía (juntadeandalucia.es)), the national network ERGNSS (National Geodetic Network of Reference Stations, Información descriptiva - Instituto Geográfico Nacional (ign.es)), the Topo-Iberia geodynamic research campaign network, Topo-Iberia: Introduction (igme.es) (Garate et al., 2015) and the IGS network Network – International GNSS Service (igs.org). 44 stations with 7 to 15 years of data (between 2007 and 2022) were considered in Andalucía and its surroundings (Fig. 1). The lowest station, CARG, is located at the coast at 8.4 m above the mean sea level, while the highest station, NEVA, is located in the Sierra Nevada mountain chain, at approximately 2880 m a.m.s.l..

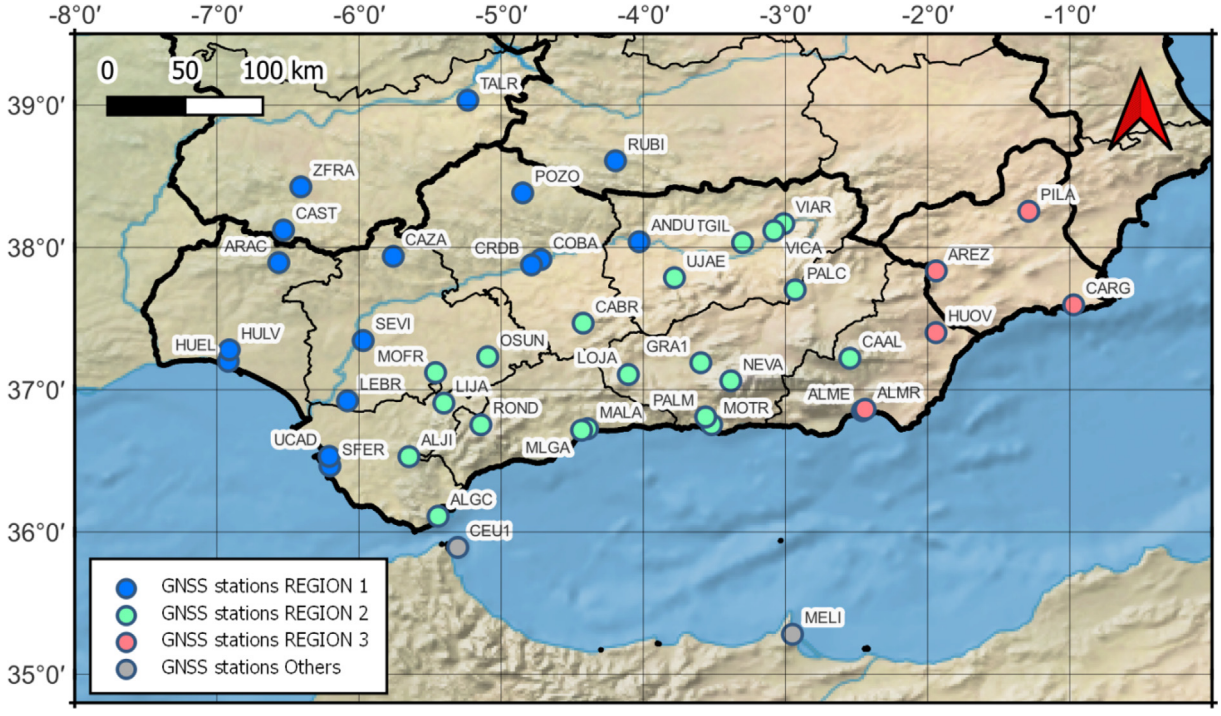

Fig. 1. GNSS stations with more than 7 years of data in Andalucía and surrounding territories (Southern Spain).

Please cite this article as: L. Retegui Schiettekatte, M. Selmira Garrido and M. Clara de Lacy, Use of GNSS and ERA5 precipitable water vapor based standardized precipitation conversion index for drought monitoring in the Mediterranean coast: A first case study in Southern Spain, Advances in Space Research, https://doi.org/10.1016/j.asr.2023.08.030

The GNSS data was processed with goGPS (Herrera Olmo et al., 2015) version 1.0. This is an open-source scientific GNSS processing software which is implemented in Matlab and has already been used for positioning and troposphere estimation purposes in other studies with satisfactory results (e.g. Barindelli et al., 2018; Ssenyunzi et al., 2019; Coletta et al., 2021; Mascitelli et al., 2021). The data was processed using the PPP (Precise Point Positioning) technique and only GPS observations in order to obtain continuous time series between the 1st of January of 2007 and the 1st of January of 2022. CODE operational final products have been used for ephemeris, clock files and Earth Rotation Parameters (Dach et al., 2016). A 7° elevation mask was applied with a satellite-elevation dependent weighting parameter. An ionosphere-free combination was used along with the application of High Order Ionosphere corrections. For the ZTD estimation, Saastamoinen model (Saastamoinen, 1972) with Global Pressure Temperature (GPT) model meteorological values (Boehm et al., 2007) were used as a priori values. Global Mapping Function (Boehm et al., 2006) and Chen & Herring gradient mapping functions (Chen and Herring, 1997) were used for troposphere mapping. A daily set of station coordinates was estimated, while the ZTD was estimated every hour and the ZTD gradients were estimated every four hours.

The GNSS time series were screened based on the vertical position time series, by discarding as outliers the datapoints that exceeded 5 times the variability of the vertical position (results of the screening are described in Section 3.1). The screened ZTD values were compared with values published by IGS and EUREF for the 8 stations belonging to at least one the two international networks (these are ALME, CARG, CEU1, COBA, HUEL, MALA, MELI, and SFER). In the case of Euref, Repro2 (Pacione et al., 2017) overlaps by 8 years (2007–2014) and, therefore, both the original Euref estimations and Repro2 were considered for validation.

2.2. ERA5 meteorological data

Conversion from GNSS-ZTD to GNSS-PWV requires of pressure and water–vapor-weighted mean atmospheric temperature data for the position of the GNSS stations. The temperature, pressure and humidity profiles extracted from "ERA5 (European Center for Medium-Range Weather Forecasts Reanalysis 5) monthly averaged data on pressure levels from 1940 to present" model (Hersbach et al., 2023) were used to compute these meteorological variables. The data was downloaded from the Copernicus Climate Change Service (C3S) Climate Data Store. In addition, ERA5-PWV was also computed from the same variables.

The vertical pressure interpolation was carried out following the procedure described by Jade and Vijayan (2008). T_m was computed using the equation given by Davis et al. (1985).

$$T_m = \frac{\int_{z_s}^{z_{top}} \frac{Pv}{T} dz}{\int_{z_s}^{z_{top}} \frac{Pv}{T^2} dz} \tag{1}$$

where T_m is the water–vapor-weighted mean temperature, T is the temperature, Pv is the water vapor pressure (hPa), and the integral must be performed over the zenith path dz, from the station height z_s to the top of the atmosphere z_{top}. The water vapor pressure was computed using equation (2)

$$Pv = \frac{q \cdot p}{\frac{M_w}{M_d} + \left(1 - \frac{M_w}{M_d}\right) q} \tag{2}$$

where $M_d = 28.9634$ g/mol is the molar mass of dry air, $M_w = 18.01528$ g/mol is the molar mass of water vapor, p is the atmospheric pressure (hPa) and q is the specific humidity (kg/kg). The water vapor pressure was necessary for the computation of PWV, which was integrated using equation (3)

$$PWV = \frac{1}{\rho_w \cdot g} \int_{p_{top}}^{p_s} q \cdot dp \tag{3}$$

where $\rho_w = 1$ kg/l is the density of water and g is the gravity value at the computation point, and p_s and p_{top} are the surface pressure and top-atmosphere pressure respectively.

Both integrations (T_m and PWV) were numerically implemented in a similar fashion to previous works, assuming a linear progression of the integrands between the vertical pressure levels of the model (e.g., W. Zhang et al., 2019; Yang et al., 2019; Y. Zhang et al., 2019). Coastal stations were sometimes found to be located under the lowest pressure level of 1000 hPa (240 m under the lowest pressure level in the most extreme case). In these cases, the pressure values were extrapolated using the formulation in Jade and Vijayan (2008), while for the mean temperature and PWV the lapse rate of the integrand was computed using the two lowest pressure levels. In this study the top of the atmosphere in the integration corresponds to the height of the highest pressure level of the model (1 hPa), which is in all moments above 45 km for the considered region and timespan.

The model has a native 0.25° × 0.25° horizontal grid resolution. Therefore, for each GNSS station, the pressure, mean temperature and PWV variables were computed for the four nearest grid points and the values at the precise GNSS station position were interpolated based on the angular distance to the grid points, following the method described in Jade and Vijayan (2008).

2.3. GNSS-PWV computation

The monthly GNSS-PWV has been computed by combining the monthly mean of Zenith Total Delay (ZTD) provided by the GNSS processing results with meteorological pressure and temperature data. First, the wet part (Zenith Wet Delay) was computed by subtracting the dry

Please cite this article as: L. Retegui Schiettekatte, M. Selmira Garrido and M. Clara de Lacy, Use of GNSS and ERA5 precipitable water vapor based standardized precipitation conversion index for drought monitoring in the Mediterranean coast: A first case study in Southern Spain, Advances in Space Research, https://doi.org/10.1016/j.asr.2023.08.030

or hydrostatic part (Zenith Hydrostatic Delay) from the total delay (ZTD):

$$\mathrm{ZWD} = \mathrm{ZTD} - \mathrm{ZHD} \tag{4}$$

The ZHD was computed by using surface pressure values in the Saastamoinen (1972) formula:

$$\mathrm{ZHD} = \frac{0.0022768\,p}{(1 - 0.00266\cos(2\phi) - 0.00000028 \times h)} \tag{5}$$

where p (hPa) is the pressure at the GNSS station, φ is the latitude and h (m) is the station's orthometric height.

The ZWD has been converted to PWV using the Askne and Nordius (1987) factor,

$$\mathrm{PWV} = Q \times \mathrm{ZWD} \tag{6}$$

$$Q = \frac{4615.24}{\left(\frac{3.739\times10^5}{T_m} + 22.1\right)} \tag{7}$$

where T_m (K) is the weighted mean temperature of the atmosphere.

The resulting PWV values have been validated against the ERA5 monthly averaged pressure level model-derived PWV estimations. The PWV computation and validation have been restricted to the Iberian Peninsula to reduce the spatial extent of the meteorological data and because precipitation data, needed for the subsequent SPCI computation, was not available for the stations located on the African continent. Hence, stations CEU1 (Ceuta) and MELI (Melilla) have been omitted from these calculations.

2.4. Precipitation, SPEI and SPI data

Precipitation data, as well as the reference drought indices' values, were extracted from the 1.1 km × 1.1 km resolution database developed by Vicente-Serrano et al. (2017). The drought indices considered in this study, that is, the Standardized Precipitation Evapotranspiration Index (SPEI) (Vicente-Serrano et al., 2010) and the Standardized Precipitation Index (SPI) (McKee et al., 1993), are openly available in https://monitordesequia.csic.es/historico/ for the area of Spain.

Both indices are multi-timescale, i.e., they can be computed for different timescales, which usually range between 1 month and 24 months. The SPI is based on the simpler Standardized Precipitation (SP) concept, which represents the difference of precipitation from the mean for a specified time period divided by the standard deviation, where the mean and standard deviation are determined from past records (McKee et al., 1993) (equation (8)).

$$\mathrm{SP}_{n,\mathrm{normal}} = \frac{\mathrm{P}_n - \bar{\mathrm{P}}_n}{\sigma_{\mathrm{P}_n}} \tag{8}$$

where $\mathrm{P_n}$ is the mean precipitation computed over a timescale of n months, and $\bar{\mathrm{P}}_n$ and σ_{P_n} are the Gaussian mean and standard deviation computed over past records with the same timescale. The additional complexity of SPI with respect to the presented SP consists of accounting for the fact that precipitation is typically not normally distributed on accumulated periods of 12-months or less. Therefore, for the SPI index computation, the records are first fitted to a non-gaussian function, usually a gamma function. More details on the computation can be found on McKee et al. (1993).

The SPEI is derived using a similar computation as for the SPI, but additionally accounts for the water balance by subtracting potential evapotranspiration to the precipitation variable (equation (9)).

$$\mathrm{D}_n = \mathrm{P}_n - \mathrm{PET}_n \tag{9}$$

where P_n, PET_n and D_n are the Precipitation, Potential Evapotranspiration and the difference between both respectively, all computed over a n-month timescale. The SPEI index is computed over the variable D_n. This allows to account for the influence of temperature in drought, which is especially relevant in the actual context of global warming Vicente-Serrano et al. (2010). More information about this index can be found on (Vicente-Serrano et al., 2010). Potential Evapotranspiration can be computed in several ways. In the case of the database used on this study it has been computed using the Penman-Monteith (PM) method (Allan et al., 1998).

For more details on the meteorological data treatment and the computation of SPI and SPEI drought indices that were used in this study, refer to Vicente-Serrano et al. (2017).

2.5. SPCI computation

The SPCI (Zhao et al., 2020) is a standardized multiscale index, based on GNSS precipitation effectiveness calculation as done by Bordi et al. (2016). The multiscale PCI (Precipitation Conversion Index) is computed in the following way:

$$\mathrm{PCI}_n = \frac{\sum_{i=m}^{m+n-1} \mathrm{P}_i^{total}}{\sum_{i=m}^{m+n-1} \mathrm{PWV}_i^{mean} \times \mathrm{day_i}} \times 100 \tag{10}$$

where P_i^{total} is the total monthly accumulated precipitation of month i, PWV_i^{mean} is the mean PWV value of month i, $\mathrm{day_i}$ is the number of days on month i, n is the number of months in the multi-month scale (in this work, $n = 1, 3, 6, 9, 12, 24$ months) and m is the first month of a multi-month scale. Hence, PCI_n represents the precipitation conversion index with a n-month scale. The index is finally standardized for inter-comparing with other indices:

$$\mathrm{SPCI}_n = nor(\mathrm{PCI}_n) = \frac{\mathrm{PCI}_n - \bar{\mathrm{PCI}}_n}{\sigma_{\mathrm{PCI}_n}} \tag{11}$$

Please cite this article as: L. Retegui Schiettekatte, M. Selmira Garrido and M. Clara de Lacy, Use of GNSS and ERA5 precipitable water vapor based standardized precipitation conversion index for drought monitoring in the Mediterranean coast: A first case study in Southern Spain, Advances in Space Research, https://doi.org/10.1016/j.asr.2023.08.030

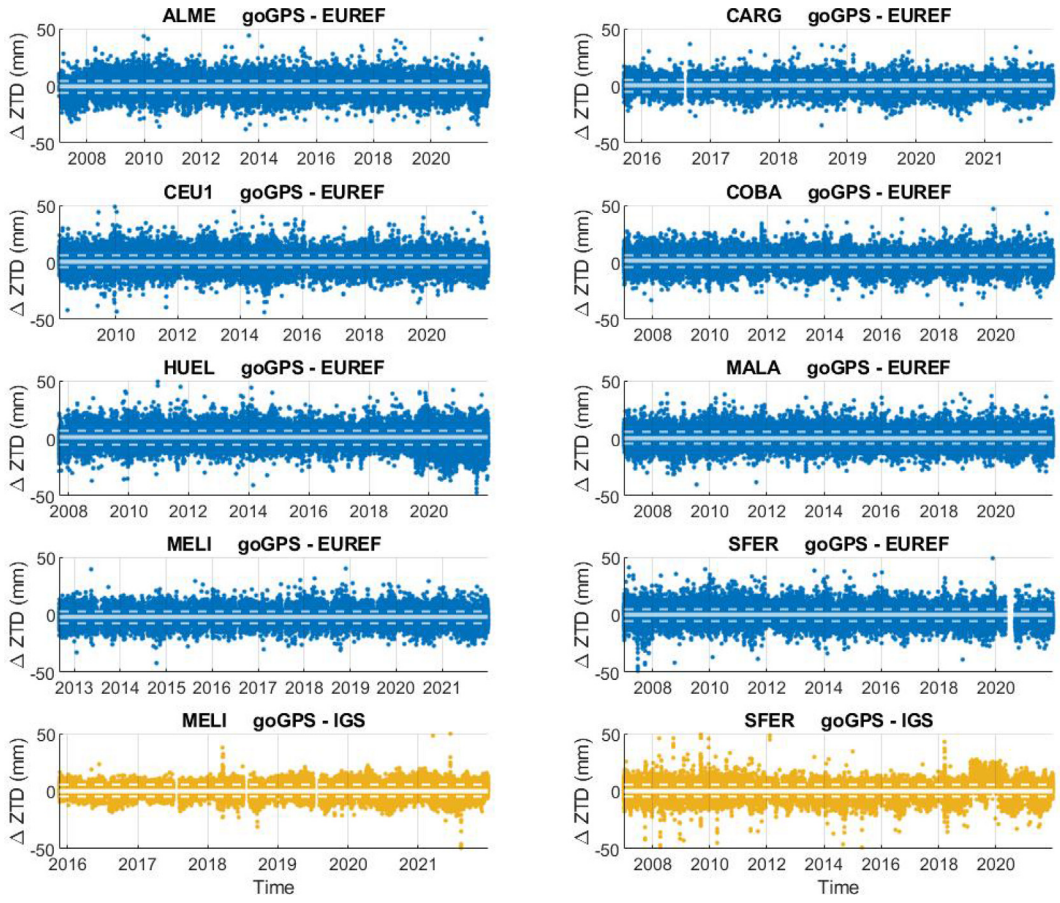

Fig. 2. Differences between goGPS ZTD and Euref/IGS ZTD products, for the 8 stations belonging to these international networks. The white horizontal lines represent the mean and standard deviation of the differences.

3. Results and discussion

3.1. Evaluation of ZTD estimation results

A basic data screening of the vertical position computed with goGPS was performed for outlier detection. As a result, for most of the stations, less than 0.06% of the data points were eliminated, except for MELI (2%), UCAD (1.9%), SFER (0.7%), NEVA (0.6%) and CAAL (0.1%) which showed more anomalies. The resulting ZTD time series were validated against IGS and EUREF hourly ZTD publications. The differences between the reference and computed ZTD time series are shown in Fig. 2. and the validation results are shown in Table 1.

SFER initially showed a high standard deviation with respect to IGS (13.5 mm) while this deviation was lower when compared to Euref (5.3 mm). This turned out to be due to some particular defective files of the IGS between the years 2011 and 2014, in which the ZTD values remain stuck around 2.3 m for a whole day, resulting in differences of up to 216 mm between IGS and goGPS or Euref. When omitting the days corresponding to these files, a lower difference of 0.4 mm $\pm$ 5.9 mm was achieved between the goGPS results and the IGS product. Some defective data was also found for MELI for days 10th of December of 2020, 19th of March, 17th of June and 12th of August of 2021, where the IGS time series displayed particularly high or low values, reaching differences up to 167 mm with respect to goGPS and Euref solutions. When omitting these four days, the standard deviation between goGPS and IGS was reduced from 6.5 mm to 5.0 mm and the mean difference from 0.5 mm to 0.4 mm. For the remaining stations, mean differences below 2 mm and standard deviations between 5 mm and 6 mm can be found, excepting MELI which shows a difference of up to -2.8 mm when compared against EUREF. These values are in the range of those found in comparisons between specific software and IGS troposphere products in previous studies (Barindelli et al., 2018; Morel et al., 2015; Sguerso et al., 2015).

3.2. GNSS-PWV and ERA5-PWV comparison

PWV time series have been computed for all of the stations located on the Southern Iberian Peninsula (42 stations, excluding CEU1 and MELI) following the methodology described in Section 2.3. For the stations located below 1500 m height, mean PWV values located in the range of 10 mm for the higher stations to 19.7 mm for sea level stations have been found. The mean PWV

Please cite this article as: L. Retegui Schiettekatte, M. Selmira Garrido and M. Clara de Lacy, Use of GNSS and ERA5 precipitable water vapor based standardized precipitation conversion index for drought monitoring in the Mediterranean coast: A first case study in Southern Spain, Advances in Space Research, https://doi.org/10.1016/j.asr.2023.08.030

Table 1
Results of the comparison between goGPS ZTD estimations and IGS/EUREF ZTD estimations. The results are expressed as the mean difference ± standard deviation.

	Mean difference (mm) ± standard deviation (mm)		
	Difference between ZTD coming from **goGPS – EUREF**	Difference between ZTD coming from **goGPS – EUREF Repro2**	Difference between ZTD coming from **goGPS – IGS**
ALME	−0.9 ± 5.5	−1.7 ± 6.0	
CARG	0.0 ± 5.0		
CEU1	0.9 ± 5.4	0.1 ± 5.9	
COBA	1.0 ± 4.9	1.2 ± 5.3	
HUEL	0.7 ± 6.0	1.2 ± 5.8	
MALA	0.2 ± 5.2	−0.2 ± 5.6	
MELI	−2.1 ± 5.1	−2.3 ± 5.4	0.4 ± 5.0
SFER	−0.6 ± 5.1	−0.4 ± 5.3	0.4 ± 5.9
Mean:	**−0.1 ± 5.3**	**−0.3 ± 5.6**	**0.4 ± 5.4**

depends linearly on the station height: it decreases by 7.3 mm with each km of altitude. For the highest stations (CAAL, Calar Alto, to 2160 m a.m.s.l. and NEVA, Sierra Nevada, to 2883 m a.m.s.l.) the PWV values deviate from the trend of the other stations due to the lower content of PWV on higher atmospheric layers.

The monthly GNSS-PWV and ERA5-PWV time series have been compared. An average mean difference of −0.3 mm has been found, with mean difference values between −1.0 mm (MELI) and 0.3 mm (HUOV and PALM). The standard deviation of the differences has an average of 0.7 mm, with values ranging from 0.3 mm (NEVA) to 1.4 mm (TGIL). As monthly (and not daily or hourly) values of PWV estimations have been compared, these differences are, as could be expected, bellow those found by other authors that compare daily values. On the daily timescale, a few millimetres differences are generally found (e.g., Li et al., 2020; Ssenyunzi et al., 2020).

Differences have also been computed between the ERA5-PWV- and GNSS-PWV-derived SPCI indices. The 1-month timescale SPCI displays very similar values for both, with an average of the absolute mean difference of 0.04 units and a standard deviation of 0.16. However, when the timescale is increased, the cumulative effect of all the differences becomes more apparent. As a result, at the 24-months timescale, the average of the mean absolute difference increases to 0.22 units, while its standard deviation is of 0.20 units.

3.3. Temperature, precipitation, and PWV correlation analysis

This paper aims to test the performance of the SPCI in a region with a low correlation level between PWV and precipitation such as Southern Spain. Hence, before starting with the SPCI computation, the correlations between

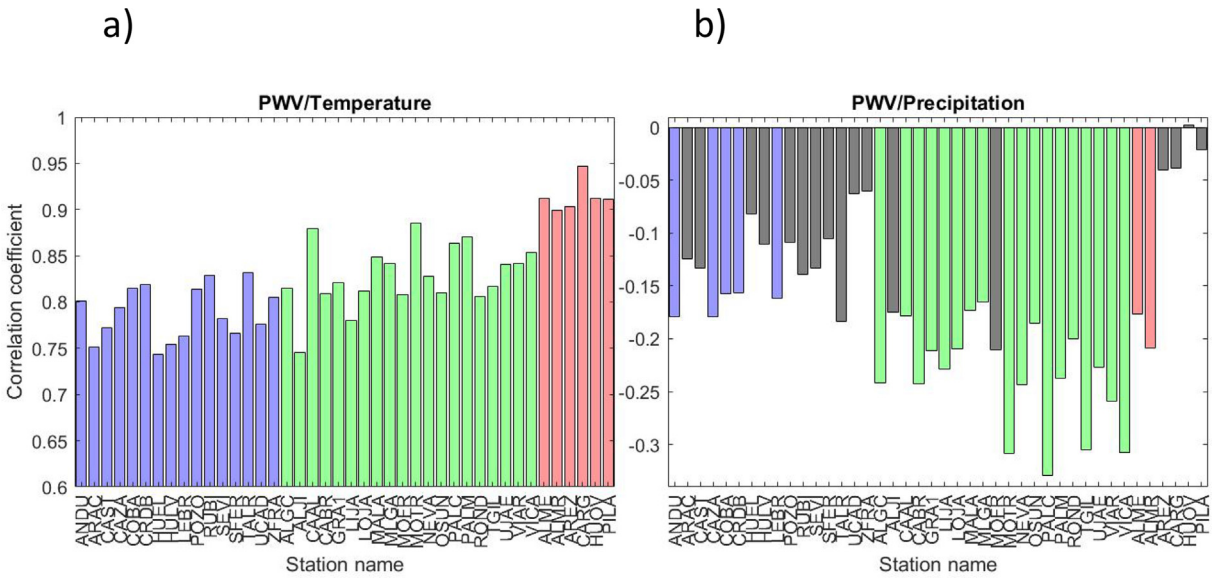

Fig. 3. Correlation coefficients between a) PWV and temperature, b) PWV and precipitation, for the different geographical areas. Blue color corresponds to region 1. Green corresponds to region 2. Red corresponds to region 3. Stations for which correlations are not significant (p-value greater than 0.05) appear masked in grey.

Please cite this article as: L. Retegui Schiettekatte, M. Selmira Garrido and M. Clara de Lacy, Use of GNSS and ERA5 precipitable water vapor based standardized precipitation conversion index for drought monitoring in the Mediterranean coast: A first case study in Southern Spain, Advances in Space Research, https://doi.org/10.1016/j.asr.2023.08.030

PWV and temperature as well as PWV and precipitation are studied in detail. These correlations have been computed and are shown in Fig. 3. The correlation levels are in general agreement with the results of Zhao et al. (2020), with high correlation levels ranging between 0.74 and 0.92 for PWV and temperature, and low (sometimes not-significative) and negative correlation levels between 0.02 and −0.53 for PWV and precipitation.

Regarding the variation of these correlation levels along the territory, the highest correlations between PWV and temperature are reached on the eastern side of the territory (region 3). In contrast, strongest and most significant negative correlation levels between PWV and precipitation are found in region 2 (Betic mountain range), suggesting that the complex orography of the territory could be influencing the relationship between PWV and precipitation.

Table 2
Average and standard deviation of the correlation coefficients between GNSS-SPCI and SPEI for stations in the three considered geographic regions.

GNSS-SPCI	Region 1		Region 2		Region 3		Total
	Mean	STD	Mean	STD	Mean	STD	Mean
1-month	0.66	0.04	0.67	0.04	0.66	0.07	**0.67**
3-months	0.83	0.02	0.81	0.05	0.83	0.02	**0.82**
6-months	0.89	0.03	0.85	0.06	0.87	0.04	**0.87**
9-months	0.91	0.03	0.87	0.06	0.88	0.05	**0.89**
12-months	0.93	0.04	0.89	0.06	0.89	0.05	**0.90**
24-months	0.93	0.05	0.89	0.09	0.88	0.07	**0.90**

Table 3
Average and standard deviation of the correlation coefficients between ERA5-SPCI (61 years) and SPEI for stations in the three considered geographic regions.

ERA5-SPCI	Region 1		Region 2		Region 3		Total
	Mean	STD	Mean	STD	Mean	STD	Mean
1-month	0.70	0.02	0.67	0.03	0.67	0.02	**0.68**
3-months	0.86	0.01	0.84	0.03	0.84	0.01	**0.85**
6-months	0.91	0.01	0.89	0.03	0.89	0.01	**0.90**
9-months	0.93	0.01	0.91	0.03	0.91	0.02	**0.92**
12-months	0.95	0.01	0.93	0.03	0.92	0.02	**0.93**
24-months	0.95	0.02	0.94	0.03	0.93	0.03	**0.94**

3.4. SPCI computation and correlation analysis

The GNSS-SPCI and ERA5-SPCI have been computed for all the stations for 6 different time scales: 1, 3, 6, 9, 12 and 24 months. The correlation coefficients with respect to SPEI have been computed and are shown in Appendix A. Mean values and standard deviations for each region, as well as for all the region, are summarized in Tables 2 and 3. In general, high correlation values are found. The correlation coefficients display mean values of 0.67 and 0.68 for the 1-month timescale, for GNSS-SPCI and ERA5-SPCI respectively. This level becomes higher as the timescale increases, reaching its maximum at the 12-month and
24-month timescales (0.90 for GNSS-SPCI and 0.93–0.94 for ERA5-SPCI). In the case of GNSS-SPCI, the correlation levels drop slightly at the 24-month timescale for some stations, while this effect is not observed in the case of ERA5-SPCI. ERA5-SPCI generally shows higher correlation levels than the GNSS-SPCI for all the timescales.

The results have been studied in more detail attending to the geographical region the stations belong to. The correlation coefficients for the 24-months timescale depending on the region are represented in Fig. 4 (a and c). One of the striking features observed for the GNSS-SPCI consists of the great variability of the correlation coefficients inside a given geographical region, which doesn't occur for ERA5-SPCI. Table 2 reveals that, for the GNSS-SPCI, the standard deviations between the correlation coefficients inside a given region increase with time and even reach 0.09 points of standard deviation in the case of region 2. Moreover, some inconsistencies can even be found between close stations in the case of GNSS-SPCI. For instance, MALA

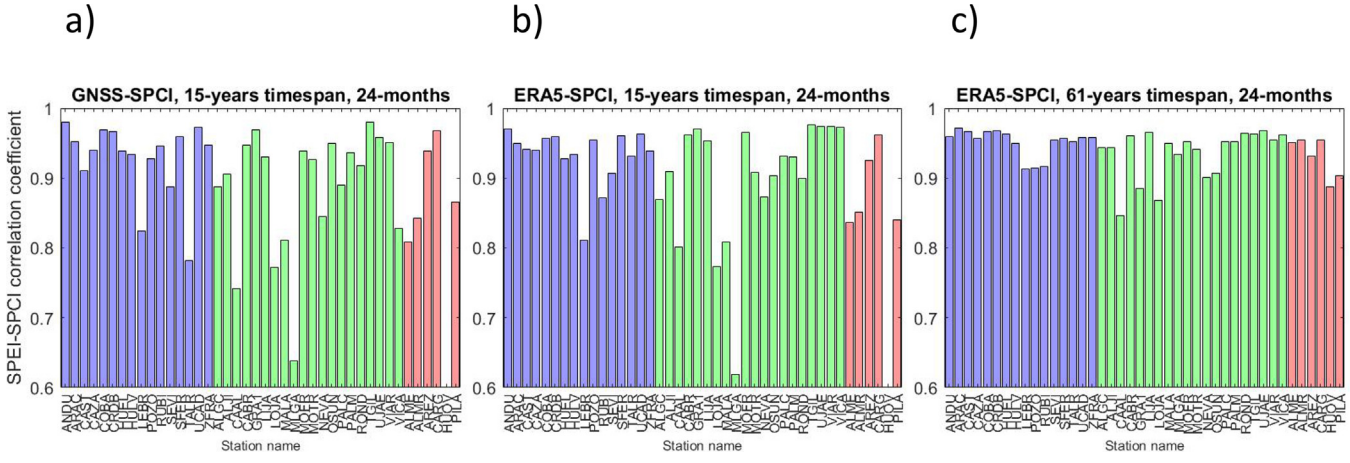

Fig. 4. SPCI-SPEI correlation coefficients for 24-month timescale, computed using a) GNSS-PWV (15 years), b) ERA5-PWV (15 years) and c) ERA-PWV (61 years). Blue color corresponds to region 1. Green corresponds to region 2. Red corresponds to region 3.

Please cite this article as: L. Retegui Schiettekatte, M. Selmira Garrido and M. Clara de Lacy, Use of GNSS and ERA5 precipitable water vapor based standardized precipitation conversion index for drought monitoring in the Mediterranean coast: A first case study in Southern Spain, Advances in Space Research, https://doi.org/10.1016/j.asr.2023.08.030

and MLGA, located at a 4 km distance, have coefficients of 0.81 and 0.64 respectively for the 24-month timescale; or VIAR and VICA (8 km distance) show coefficients of 0.95 and 0.83 respectively for the same timescale. In addition, the station HUOV shows a very singular behaviour with respect to the other stations belonging to region 3, with very low correlation coefficients, reaching 0.14 for the 24-month timescale (this station has been omitted from the mean correlation computations as an outlier).

One of the main differences between the GNSS-SPCI and ERA5-SPCI is the timespan of the time series (15 years and 61 years, respectively). In order to explore the possible influence of this factor in the aforementioned incoherencies, the ERA5-SPCI has been recomputed over a similar time period as the GNSS time series, that is, 2007–2022. The obtained correlation coefficients for the 24-month timescale are represented on Fig. 4 b.

For this new ERA5-SPCI (15 years), incoherencies also appear for the stations MALA-MLGA and HUOV. As a consequence, these can be attributed to an insufficient length of the data time series. Fig. 5 presents the ERA5-PWV, precipitation, ERA5-PCI and ERA5-SPCI (24-month timescale) time series for the 15-years computation for stations MALA and MLGA, two GNSS stations very close to each other (the distance between them is less than 4 km and the difference in altitude is above 4 m). It can be seen that, although the differences in ERA5-PWV and precipitation are very small between both stations, the drought indices show more important differences. These differences can be explained by the use of the 24-month timescale, which causes an accumulation of all the small differences in PWV and precipitation over two years, amplifying them in the drought index time series. This also explains the fact that the standard deviation of the correlation coefficients inside a region increases when the drought index timescale is increased, as seen in Table 2. Table 3 shows that, when using 61 years time series, this effect is less notorious, since the correlation levels display lower standard deviations that are independent of the timescale.

As far as VICA and VIAR stations are concerned, the differences between them disappear when using the 15-years ERA5-SPCI time series. Hence, the original incoherency is attributed to the very short timespan of the GNSS VICA time series, which only covers 8 years. As a consequence, the short timespan of the GNSS data (7–15 years in this study) appears to be an inconvenience for the right computation of the SPCI time series and therefore should be addressed or considered when analyzing the GNSS-SPCI performance. The ERA5-PWV data seems to solve this problem by introducing long and continuous PWV time series. It is true that, as long as ERA5 is a model, its smoothness and its limited spatial resolution (0.25° × 0.25°, approximately 30 km × 30 km in Southern Spain) could be a disadvantage when trying to study the spatial variability of SPCI in a territory with a complex orography such as Southern Spain. However, when SPCI is computed, ERA5-PWV is combined with precipitation data with a higher resolution (1 km × 1 km). Therefore, the possible influence of the smoothness and coarse resolution of ERA5-PWV in the SPCI should be studied in more detail in view of the eventual use of this type of data for SPCI time series estimation.

Under the more coherent results of ERA5-SPCI, it can be seen that the best agreement between SPCI and SPEI can be found for region 1. Fig. 4.c shows that some stations still deviate from the mean tendency corresponding to this

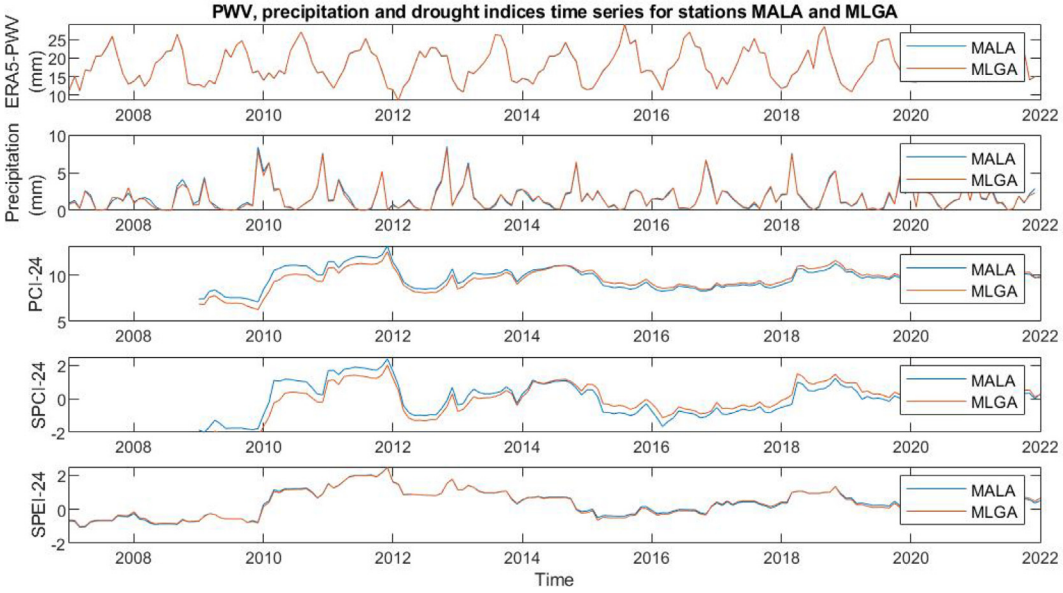

Fig. 5. PWV, precipitation and drought indices time series for stations MALA and MLGA. Although the differences in precipitation are very low, when accumulated over 24-months (2 years) these cause important differences in the SPCI between the two stations, resulting in very different correlation coefficients with respect to SPEI.

Please cite this article as: L. Retegui Schiettekatte, M. Selmira Garrido and M. Clara de Lacy, Use of GNSS and ERA5 precipitable water vapor based standardized precipitation conversion index for drought monitoring in the Mediterranean coast: A first case study in Southern Spain, Advances in Space Research, https://doi.org/10.1016/j.asr.2023.08.030

region: these are LEBR, POZO and RUBI, which show a correlation level around 0.92 for the 24-month timescale in contrast to the other stations of the region, with correlation coefficients higher than 0.95. The three of them are located in the most mountainous areas among the stations of region 1. In region 2, where the topography is very irregular, the variability of the correlation coefficients is greater (0.03 points of correlation coefficient standard deviation independently of the timescale). An intermediate variability degree is found in region 3 where the topography is quite irregular too. All this seems to indicate that the SPCI estimates show slightly less agreement with SPEI for many of the stations located in the mountainous regions.

3.5. Comparison with other global results

The correlation coefficients obtained in this study are compared to the worldwide results obtained by Zhao et al. (2020). The worldwide results are based on the computation of GNSS-SPCI time series using IGS ZTD products starting from 2005 to 2016 (12-year timespan), as well as ERA-Interim-SPCI time series for the global mainland for the 1979–2015 period (37 years). Table 4 shows the percentage of locations on the global mainland with correlation coefficients greater than 0.8 at different month scales, both for Zhao et al. (2020) and the stations considered in the present study.

For low time scales, the SPCI performs better in Southern Spain compared to the general global performance. For instance, for the 3-month time scale, while only about 15% of the world mainland shows a correlation greater than 0.8, more than 70% of the GNSS stations of this study reach this threshold (90% if ERA5 61-year time series is used). For the 9-month time scale, the percentage is around 50% for the global mainland and 95% to 100% for Southern Spain. The trends become more similar for the 12-month and 24-months timescales. When the time scale is increased to 12 months, the global trend increases significantly to 96–98% of the stations with high correlations, and this trend slightly drops for the 24-months timescale. In the case of Southern Spain, the statistics drop at 12- and 24-months timescale for the GNSS data, but remain high for the SPCI computed using ERA5 61-year time series.

These correlation coefficients can also be compared to more local results. Ma et al. (2021) and Zhao et al. (2022) study the correlation between SPEI and SPCI for different stations in Yunnan, China. This region is described as an arid area, while Southern Spain is generally considered a semi-arid area. The correlation coefficient values achieved by Ma et al. (2021) for the 12-months timescale are similar to the ones obtained in this study, in the range of 0.89 to 0.97. Zhao et al. (2022) achieve lower values, between 0.85 and 0.90, for the same region, possibly due to the shorter timespan of their time series (8 years). As for the variation of the correlation coefficients depending on the timescale, in Ma et al. (2021) they seem to follow similar trends as the GNSS-SPCI correlations in this study, although the correlations levels are slightly higher for the 1-month timescale in the case of Yunnan.

Zhao et al. (2020) also test the GNSS-SCPI at the IGS FAIR station (Fairbanks, USA). In this case, the presented correlation coefficients, starting at 0.93 on the 1-month timescale and reaching 0.98 on the 24-month timescale, are much higher than those obtained in this study.

In conclusion, the SPCI-SPEI correlation levels in Southern Spain can be considered high when compared to global mainland correlation levels, especially for low timescales. This result implies that, despite the atypical precipitation-PWV correlation, the SPCI can perform satisfactorily and has an interesting potential for drought monitoring in this region. These suggest that the SPCI could be an interesting index for drought studies in the Mediterranean area, although the results cannot be generalized due to the spatial variability that exists in this territory, and the index should be tested in more Mediterranean regions.

3.6. Performance of SPCI vs. SPI

In the previous sections the good performance of the SPCI in Southern Spain has been shown with respect to the SPEI, which accounts for both precipitation and evapotranspiration. The last question that is addressed in this study is the following: does the computation of SPCI, based on precipitation and PWV data, constitute any improvement with respect to SPI time series, which are only based on precipitation data? To answer this question,

Table 4
Percent of stations / locations with a correlation coefficient with SPEI greater than 0.8 for different time-scales. The global results have been taken from Zhao et al. (2020).

	Correlation coefficients > 0.8			
	Global results		**Southern Spain results**	
	GNSS-SPCI(%)	**ERA-Interim-SPCI(%)**	**GNSS-SPCI(%)**	**ERA5-SPCI(%)**
3 months	15.38	14.35	73.2	97.6
6 months	21.50	20.94	92.7	100
9 months	53.63	51.35	95.1	100
12 months	97.90	96.06	92.7	100
24 months	96.84	95.26	90.2	100

Please cite this article as: L. Retegui Schiettekatte, M. Selmira Garrido and M. Clara de Lacy, Use of GNSS and ERA5 precipitable water vapor based standardized precipitation conversion index for drought monitoring in the Mediterranean coast: A first case study in Southern Spain, Advances in Space Research, https://doi.org/10.1016/j.asr.2023.08.030

Table 5
Correlation coefficient of ERA5-SPCI and SPI time series with respect to SPEI for different timescales. Cases in which SPCI outperforms SPI are highlighted.

	6-months		12-months		24-months	
	SPI	SPCI	SPI	SPCI	SPI	SPCI
ALGC	0.98	0.89	0.99	0.93	0.98	0.94
ALJI	0.98	0.89	0.99	0.93	0.99	0.94
ALME	0.92	0.90	0.91	**0.93**	0.90	**0.95**
ALMR	0.93	0.91	0.91	**0.94**	0.90	**0.95**
ANDU	0.95	0.91	0.96	0.95	0.94	**0.96**
ARAC	0.98	0.92	0.99	0.96	0.99	0.97
AREZ	0.94	0.90	0.94	0.92	0.92	**0.93**
CAAL	0.96	0.81	0.96	0.83	0.96	0.85
CABR	0.97	0.91	0.98	0.95	0.98	0.96
CARG	0.95	0.91	0.95	0.93	0.95	**0.95**
CAST	0.98	0.92	0.99	0.96	0.98	0.97
CAZA	0.97	0.91	0.99	0.95	0.98	0.96
COBA	0.96	0.91	0.98	0.96	0.96	**0.97**
CRDB	0.96	0.91	0.98	0.96	0.96	**0.97**
GRA1	0.95	0.88	0.95	0.90	0.95	0.88
HUEL	0.96	0.90	0.98	0.96	0.98	0.96
HULV	0.96	0.90	0.98	0.95	0.98	0.95
HUOV	0.95	0.88	0.95	0.88	0.93	0.89
LEBR	0.96	0.88	0.97	0.92	0.97	0.91
LIJA	0.98	0.90	0.99	0.95	0.99	0.97
LOJA	0.97	0.87	0.98	0.88	0.98	0.87
MALA	0.96	0.88	0.98	0.94	0.97	0.95
MLGA	0.96	0.87	0.97	0.92	0.97	0.93
MOFR	0.96	0.91	0.98	0.95	0.98	0.95
MOTR	0.97	0.89	0.97	0.93	0.97	0.94
NEVA	0.98	0.85	0.98	0.88	0.98	0.90
OSUN	0.97	0.87	0.98	0.90	0.98	0.91
PALC	0.96	0.92	0.96	0.94	0.95	0.95
PALM	0.97	0.89	0.98	0.94	0.97	0.95
PILA	0.95	0.87	0.95	0.89	0.93	0.90
POZO	0.96	0.90	0.97	0.93	0.95	0.91
ROND	0.98	0.91	0.99	0.95	0.99	0.96
RUBI	0.95	0.90	0.96	0.92	0.94	0.92
SEVI	0.96	0.90	0.97	0.95	0.97	0.95
SFER	0.96	0.90	0.98	0.95	0.98	0.96
TALR	0.96	0.92	0.97	0.95	0.96	0.95
TGIL	0.96	0.92	0.96	0.95	0.95	**0.96**
UCAD	0.96	0.90	0.98	0.95	0.98	0.96
UJAE	0.95	0.92	0.96	0.96	0.95	**0.97**
VIAR	0.95	0.92	0.95	0.94	0.92	**0.95**
VICA	0.95	0.92	0.95	0.95	0.93	**0.96**
ZFRA	0.96	0.92	0.97	0.95	0.96	0.96

the SPI correlation coefficient values have been computed with respect to SPEI for the 6-, 12-, and 24-month timescales and have been compared to those obtained with ERA5-SPCI. The results are presented in Table 5.

As the results show, for the 6-months timescale the SPI presents a better performance. When the timescale is increased to 12-months, the two stations located at Almería (ALME and ALMR) show a better performance when SPCI is used with respect to SPI. However, the biggest contributions of the SPCI can be seen at the 24-months timescale. For this timescale, for 10 of the 42 considered stations the SPCI shows higher correlations with SPEI than the SPI. These stations are: ALME, ALMR, ANDU, AREZ, COBA, CRDB, TGIL, UJAE, VIAR, and VICA. All these stations are located in the same particular region, at both sides of the easternmost part of the Baetic Mountain Ranges and show rather high SPCI correlation values. The nearby station PALC also shows very similar correlation coefficients for SPCI and SPI (0.9541 and 0.9539 respectively). In contrast, the nearby station CAAL shows much lower correlations. The height of this station could be a factor influencing the lower correlation level of the SPCI estimates.

The fact that the 24-months SPCI estimations are better than the SPI for the stations belonging to a given geographical area suggests that the inclusion of PWV data in drought indices computation can really bring an improvement on drought monitoring in some cases, and hence constitute a promising data for this purpose. The ways in which this data could improve and contribute to drought monitoring can be diverse, as reflected by the different applications mentioned in Section 1 (Introduction), and is yet to be studied in depth.

4. Conclusions

The aim of this article is to test the performance of the SPCI in the region of Southern Spain. This region consists of an interesting area, on the one hand, due to the atypically low correlation levels that exist between precipitation and PWV data and, on the other hand, due to the steep topography and high climatological variability of this territory.

The GNSS observations of 44 permanent geodetic receivers have been processed to compute 7 to 15-year GNSS-ZTD values between 2007 and 2022. For this purpose, a PPP solution has been computed using the open-source goGPS software. The goGPS ZTD values have been validated against IGS and Euref ZTD products, obtaining a few millimeters level mean differences and standard deviations around 5–6 mm. ERA5-derived pressure and mean temperature values have been used to compute the PWV from the ZTD. ERA5-PWV values were also extracted and used to validate to GNSS-PWV: a mean difference of −0.3 mm and a standard deviation of 0.7 mm have been found between the PWV derived from the two datasets.

SPCI time series were calculated using the GNSS-PWV and ERA5-PWV time series and precipitation data, and were assessed by computing the correlation coefficients taking SPEI time series as a reference. In general, high correlation coefficients were found, with a mean value of 0.67–0.68 for the 3-month timescale and increasing to a mean value over 0.90 for the 12- and 24-month timescale. The use of GNSS-SPCI time series have led to some incoherencies due to the short timespan of the GNSS time series (7 to 15 years). The use of a longer timespan (61-years), allowed by ERA5-PWV data, have solved this problem providing more coherent results. Therefore, the use of ERA5 PWV for SPCI estimation has shown to constitute a very interesting option that can help to overcome prob-

Please cite this article as: L. Retegui Schiettekatte, M. Selmira Garrido and M. Clara de Lacy, Use of GNSS and ERA5 precipitable water vapor based standardized precipitation conversion index for drought monitoring in the Mediterranean coast: A first case study in Southern Spain, Advances in Space Research, https://doi.org/10.1016/j.asr.2023.08.030

lems linked to the short timespan of GNSS observations. The spatial resolution and the ability to account for the spatial variability of the ERA5-SPCI (obtained by combining ERA5-PWV and higher resolution precipitation data) remains unaddressed.

A geographical analysis of the results has been performed. In general, the highest agreement between SPCI and SPEI seems to be found in the flattest areas of the region, that is, the basin of the main river Guadalquivir, reaching correlation levels greater than 0.95 for the 24-month timescale. For more mountainous areas, the correlations still remain high but become more variable, varying between 0.85 and 0.95 for the 24-months timescale depending on the station.

When compared to global mainland results, the correlation levels found in this study have turned out to be high, especially for low timescales where the correlation values reach mean values of 0.82 and 0.85 (3-month timescale) and 0.87 and 0.90 (6-month timescale) when using GNSS and ERA5 PWV values, respectively, while global correlation coefficients remain much lower. This is the first time that SPCI is tested and studied specifically in an area with atypically low correlations between PWV and precipitation and proves that the SPCI can also have a good performance in this kind of region.

Finally, the performance of the ERA5-SPCI was compared with that of the SPI keeping the SPEI as a reference. While for low timescales the SPI performs better, for the 24-month timescale the SPCI has shown to outperform the SPI for a given region in the eastern part of the Baetic Mountains Ranges. This result suggests that the PWV data can really bring an improvement on precipitation-based drought estimation for some geographical territories and is worth to be considered and further investigated.

Declaration of Competing Interest

The authors declare that they have no known competing financial interests or personal relationships that could have appeared to influence the work reported in this paper.

Acknowledgements

This study was funded by the Junta de Andalucía (Andalusian Plan of Research, Development and Innovation, PAIDI2020 – Project P20_00897, which is a project funded by the FEDER founds, and Research Group RNM282) and by the University of Jaén (Operative Program FEDER Andalucía 2014-2020 - Project 1263446, POAIUJA 2021-2022 and CEACTEMA, Center for Advanced Studies on Earth Sciences, Energy and Environment).

The GNSS data used for this study were provided by the following institutions: Institute of Statistics and Cartography of Andalucía (IECA) of the Junta de Andalucía; National Geographic Institute of Spain (IGN); Online Archives of the Crustal Dynamics Data Information System (CDDIS), NASA Goddard Space Flight Center, Greenbelt, MD, USA. The ERA5 data (Hersbach et al., 2023) were downloaded from the Copernicus Climate Change Service (C3S) Climate Data Store. The precipitation data was kindly provided by Sergio M. Vicente-Serrano and the SPEI and SPI data was downloaded from https://monitordesequia.csic.es/historico/, all of them belonging to the database described in Vicente Serrano et al. (2017).

Appendix A. Correlation coefficients of GNSS-SPCI and ERA5-SPCI (61 years) with respect to SPEI.

(See Tables A1 and A2).

Table A1
Correlation coefficients between 15-years GNSS-SPCI and SPEI for different month scales. All correlations show a high significance level with *p-value* less than 0.05, excepting HUOV for the 24-months timescale, which has been excluded from the mean*.

GNSS-SPCI	1-m	3-m	6-m	9-m	12-m	24-m
ALGC	0.66	0.81	0.85	0.89	0.90	0.89
ALJI	0.73	0.84	0.88	0.90	0.92	0.91
ALME	0.68	0.81	0.83	0.82	0.82	0.81
ALMR	0.69	0.80	0.82	0.84	0.86	0.84
ANDU	0.68	0.87	0.93	0.95	0.96	0.98
ARAC	0.65	0.84	0.90	0.91	0.94	0.95
AREZ	0.71	0.86	0.91	0.92	0.93	0.94
CAAL	0.62	0.69	0.69	0.71	0.77	0.74
CABR	0.67	0.83	0.88	0.89	0.91	0.95
CARG	0.53	0.85	0.91	0.93	0.92	0.97
CAST	0.66	0.82	0.88	0.90	0.94	0.91
CAZA	0.69	0.84	0.90	0.92	0.93	0.94
COBA	0.68	0.83	0.89	0.92	0.94	0.97
CRDB	0.67	0.82	0.89	0.91	0.94	0.97
GRA1	0.69	0.83	0.91	0.94	0.94	0.97
HUEL	0.58	0.80	0.87	0.90	0.92	0.94
HULV	0.58	0.80	0.86	0.90	0.91	0.93
HUOV*	0.68	0.77	0.71	0.59	0.49	*0.14*
LEBR	0.69	0.80	0.82	0.82	0.82	0.82
LIJA	0.73	0.86	0.93	0.94	0.96	0.93
LOJA	0.67	0.74	0.78	0.79	0.74	0.77
MALA	0.60	0.77	0.83	0.86	0.86	0.81
MLGA	0.61	0.76	0.79	0.80	0.79	0.64
MOFR	0.68	0.79	0.82	0.84	0.91	0.94
MOTR	0.64	0.77	0.82	0.84	0.87	0.93
NEVA	0.64	0.78	0.81	0.83	0.85	0.84
OSUN	0.64	0.79	0.87	0.89	0.91	0.95
PALC	0.69	0.80	0.83	0.86	0.87	0.89
PALM	0.69	0.84	0.89	0.90	0.93	0.94
PILA	0.69	0.83	0.87	0.90	0.90	0.87
POZO	0.66	0.84	0.92	0.93	0.94	0.93
ROND	0.69	0.86	0.90	0.93	0.94	0.92
RUBI	0.66	0.86	0.90	0.92	0.94	0.95
SEVI	0.63	0.81	0.88	0.89	0.91	0.89
SFER	0.68	0.84	0.88	0.92	0.95	0.96
TALR	0.65	0.85	0.85	0.84	0.88	0.78
TGIL	0.73	0.88	0.92	0.95	0.96	0.98
UCAD	0.64	0.82	0.91	0.95	0.96	0.97
UJAE	0.72	0.88	0.92	0.95	0.96	0.96
VIAR	0.75	0.89	0.93	0.94	0.94	0.95
VICA	0.66	0.79	0.81	0.83	0.84	0.83
ZFRA	0.71	0.86	0.93	0.92	0.95	0.95
Mean*	**0.67**	**0.82**	**0.87**	**0.89**	**0.90**	**0.90**

Please cite this article as: L. Retegui Schiettekatte, M. Selmira Garrido and M. Clara de Lacy, Use of GNSS and ERA5 precipitable water vapor based standardized precipitation conversion index for drought monitoring in the Mediterranean coast: A first case study in Southern Spain, Advances in Space Research, https://doi.org/10.1016/j.asr.2023.08.030

Table A2
Correlation coefficients between 61-years ERA5-SPCI and SPEI for different month scales. All correlations show a high significance level with *p-value* less than 0.05.

ERA5-SPCI	1-m	3-m	6-m	9-m	12-m	24-m
ALGC	0.67	0.84	0.89	0.92	0.93	0.94
ALJI	0.66	0.84	0.89	0.92	0.93	0.94
ALME	0.69	0.85	0.90	0.92	0.93	0.95
ALMR	0.70	0.85	0.91	0.92	0.94	0.95
ANDU	0.71	0.86	0.91	0.93	0.95	0.96
ARAC	0.70	0.87	0.92	0.95	0.96	0.97
AREZ	0.67	0.85	0.90	0.92	0.92	0.93
CAAL	0.59	0.78	0.81	0.82	0.83	0.85
CABR	0.69	0.86	0.91	0.93	0.95	0.96
CARG	0.64	0.84	0.91	0.92	0.93	0.95
CAST	0.72	0.88	0.92	0.95	0.96	0.97
CAZA	0.71	0.86	0.91	0.94	0.95	0.96
COBA	0.71	0.86	0.91	0.94	0.96	0.97
CRDB	0.71	0.86	0.91	0.94	0.96	0.97
GRA1	0.68	0.84	0.88	0.90	0.90	0.88
HUEL	0.67	0.85	0.90	0.94	0.96	0.96
HULV	0.67	0.84	0.90	0.93	0.95	0.95
HUOV	0.69	0.84	0.88	0.88	0.88	0.89
LEBR	0.69	0.84	0.88	0.91	0.92	0.91
LIJA	0.66	0.85	0.90	0.94	0.95	0.97
LOJA	0.65	0.83	0.87	0.87	0.88	0.87
MALA	0.66	0.82	0.88	0.92	0.94	0.95
MLGA	0.66	0.81	0.87	0.90	0.92	0.93
MOFR	0.69	0.86	0.91	0.93	0.95	0.95
MOTR	0.64	0.81	0.89	0.92	0.93	0.94
NEVA	0.65	0.82	0.85	0.87	0.88	0.90
OSUN	0.65	0.83	0.87	0.89	0.90	0.91
PALC	0.71	0.88	0.92	0.93	0.94	0.95
PALM	0.65	0.82	0.89	0.92	0.94	0.95
PILA	0.65	0.83	0.87	0.89	0.89	0.90
POZO	0.69	0.87	0.90	0.92	0.93	0.91
ROND	0.68	0.85	0.91	0.94	0.95	0.96
RUBI	0.69	0.87	0.90	0.91	0.92	0.92
SEVI	0.67	0.84	0.90	0.93	0.95	0.95
SFER	0.68	0.85	0.90	0.93	0.95	0.96
TALR	0.70	0.88	0.92	0.94	0.95	0.95
TGIL	0.73	0.88	0.92	0.94	0.95	0.96
UCAD	0.70	0.85	0.90	0.93	0.95	0.96
UJAE	0.71	0.87	0.92	0.94	0.96	0.97
VIAR	0.73	0.88	0.92	0.93	0.94	0.95
VICA	0.73	0.88	0.92	0.94	0.95	0.96
ZFRA	0.73	0.88	0.92	0.94	0.95	0.96
Mean	**0.68**	**0.85**	**0.90**	**0.92**	**0.93**	**0.94**

References

Allan, R., Pereira, L., Smith, M., 1998. Crop evapotranspiration-Guidelines for computing crop water requirements-FAO Irrigation and drainage paper 56.

Askne, J., Nordius, H., 1987. Estimation of tropospheric delay for microwaves from surface weather data. Radio Sci. 22, 379–386. https://doi.org/10.1029/RS022i003p00379.

Barindelli, S., Realini, E., Venuti, G., Fermi, A., Gatti, A., 2018. Detection of water vapor time variations associated with heavy rain in northern Italy by geodetic and low-cost GNSS receivers. Earth Planets Space 70, 28. https://doi.org/10.1186/s40623-018-0795-7.

Boehm, J., Niell, A., Tregoning, P., Schuh, H., 2006. Global Mapping Function (GMF): A new empirical mapping function based on numerical weather model data. Geophys. Res. Lett. 33. https://doi.org/10.1029/2005GL025546.

Boehm, J., Heinkelmann, R., Schuh, H., 2007. Short Note: A global model of pressure and temperature for geodetic applications. J. Geod. 81, 679–683. https://doi.org/10.1007/s00190-007-0135-3.

Bordi, I., Raziei, T., Pereira, L.S., Sutera, A., 2015. Ground-based GPS measurements of precipitable water vapor and their usefulness for hydrological applications. Water Resour. Manag. 29, 471–486. https://doi.org/10.1007/s11269-014-0672-5.

Bordi, I., Zhu, X., Fraedrich, K., 2016. Precipitable water vapor and its relationship with the Standardized Precipitation Index: ground-based GPS measurements and reanalysis data. Theor. Appl. Climatol. 123, 263–275. https://doi.org/10.1007/s00704-014-1355-0.

Chen, G., Herring, T.A., 1997. Effects of atmospheric azimuthal asymmetry on the analysis of space geodetic data. J. Geophys. Res. Solid Earth 102, 20489–20502. https://doi.org/10.1029/97JB01739.

Coletta, V., Mascitelli, A., Bonazza, A., Ciarravano, A., Federico, S., Prestileo, F., Torcasio, R.C., Dietrich, S., 2021. Multi-instrumental Analysis of the Extreme Meteorological Event Occurred in Matera (Italy) on November 2019, in: Computational Science and Its Applications – ICCSA 2021: 21st International Conference, Cagliari, Italy, September 13–16, 2021, Proceedings, Part VIII. Springer-Verlag, Berlin, Heidelberg, pp. 140–154. https://doi.org/10.1007/978-3-030-87010-2_10.

Dach, R., Schaer, S., Arnold, D., Orliac, E., Prange, L., Susnik, A., Villiger, A., Jäggi, A., 2016. CODE final product series for the IGS [WWW Document]. Dach, Rolf; Schaer, Stefan; Arnold, Daniel; Orliac, Etienne; Prange, Lars; Susnik, Andreja; Villiger, Arturo; Jäggi, Adrian (2016). CODE final product series for the IGS. Astronomical Institute, University of Bern. URL http://www.aiub.unibe.ch/download/CODE (accessed 7.8.23).

Davis, J.L., Herring, T.A., Shapiro, I.I., Rogers, A.E.E., Elgered, G., 1985. Geodesy by radio interferometry: Effects of atmospheric modeling errors on estimates of baseline length. Radio Sci. 20, 1593–1607. https://doi.org/10.1029/RS020i006p01593.

Garate, J., Martin-Davila, J., Khazaradze, G., Echeverria, A., Asensio, E., Gil, A.J., de Lacy, M.C., Armenteros, J.A., Ruiz, A.M., Gallastegui, J., Alvarez-Lobato, F., Ayala, C., Rodríguez-Caderot, G., Galindo-Zaldívar, J., Rimi, A., Harnafi, M., 2015. Topo-Iberia project: CGPS crustal velocity field in the Iberian Peninsula and Morocco. GPS Solut 19, 287–295. https://doi.org/10.1007/s10291-014-0387-3.

Gu, L., Chen, J., Yin, J., Sullivan, S.C., Wang, H.-M., Guo, S., Zhang, L., Kim, J.-S., 2020. Projected increases in magnitude and socioeconomic exposure of global droughts in 1.5 and 2°C warmer climates. Hydrol. Earth Syst. Sci. 24, 451–472. https://doi.org/10.5194/hess-24-451-2020.

Herrera Olmo, A., Suhandri, H., Realini, E., Reguzzoni, M., de Lacy, M. C., 2015. goGPS: open-source MATLAB software. GPS Solutions 20, 1–9. https://doi.org/10.1007/s10291-015-0469-x.

Hersbach, H., Bell, B., Berrisford, P., Biavati, G., Horányi, A., Munoz-Sabater, J., Nicolas, J., Peubey, C., Radu, R., Rozum, I., Schepers, D., Simmons, A., Soci, C., Dee, D., Thépaut, J.-N., 2023. ERA5 monthly averaged data on pressure levels from 1979 to present. Copernicus Climate Change Service (C3S) Climate Data Store (CDS). https://doi.org/10.24381/CDS.6860A573.

Jade, S., Vijayan, M.S.M., 2008. GPS-based atmospheric precipitable water vapor estimation using meteorological parameters interpolated from NCEP global reanalysis data. J. Geophys. Res. Atmos. 113. https://doi.org/10.1029/2007JD008758.

Jiang, W., Yuan, P., Chen, H., Cai, J., Li, Z., Chao, N., Sneeuw, N., 2017. Annual variations of monsoon and drought detected by GPS: A case study in Yunnan, China. Sci. Rep. 7, 5874. https://doi.org/10.1038/s41598-017-06095-1.

Li, H., Choy, S., Wang, X., Zhang, K., Jiang, C., Li, L., Liu, X., Hu, A., Wu, S., Zhu, D., 2022. Estimation of diurnal-provided potential evapotranspiration using GNSS and meteorological products. Atmos. Res. 280, 106424. https://doi.org/10.1016/j.atmosres.2022.106424.

Li, Z.W., Tang, C.Z., Tang, S.H., Zhang, Y., 2020. COMPARISON OF GNSS PWV AND ERA5-DERIVED PWV BASED ON GNSS PWV

Please cite this article as: L. Retegui Schiettekatte, M. Selmira Garrido and M. Clara de Lacy, Use of GNSS and ERA5 precipitable water vapor based standardized precipitation conversion index for drought monitoring in the Mediterranean coast: A first case study in Southern Spain, Advances in Space Research, https://doi.org/10.1016/j.asr.2023.08.030

IN HONG KONG, CHINA. The International Archives of the Photogrammetry, Remote Sensing and Spatial Information Sciences XLII-3-W10, 987–993. https://doi.org/10.5194/isprs-archives-XLII-3-W10-987-2020.

Ma, X., Yao, Y., Zhao, Q., 2021. Regional GNSS-Derived SPCI: Verification and Improvement in Yunnan, China. Remote Sens. 13, 1918. https://doi.org/10.3390/rs13101918.

Mascitelli, A., Federico, S., Torcasio, R.C., Dietrich, S., 2021. Assimilation of GPS Zenith Total Delay estimates in RAMS NWP model: Impact studies over central Italy. Advances in Space Research, Scientific and Fundamental Aspects of GNSS - Part 2 68, 4783–4793. https://doi.org/10.1016/j.asr.2020.08.031

McKee, T.B., Doesken, N.J., Kleist, J., 1993. The relationship of drought frequency and duration to time scales. Preprints, Eighth Conf. on Applied Climatology. Anaheim, CA, Amer. Meteor. Soc., 179–184

Morel, L., Pottiaux, E., Durand, F., Fund, F., Boniface, K., de Oliveira, P.S., Van Baelen, J., 2015. Validity and behaviour of tropospheric gradients estimated by GPS in Corsica. Advances in Space Research 55, 135–149. https://doi.org/10.1016/j.asr.2014.10.004.

Ortiz de Galisteo, J.P., Cachorro, V., Toledano, C., Torres, B., Laulainen, N., Bennouna, Y., de Frutos, A., 2011. Diurnal cycle of precipitable water vapor over Spain. Q. J. R. Meteorolog. Soc. 137, 948–958. https://doi.org/10.1002/qj.811.

Ortiz de Galisteo, J.P., Bennouna, Y., Toledano, C., Cachorro, V., Romero, P., Andrés, M.I., Torres, B., 2014. Analysis of the annual cycle of the precipitable water vapour over Spain from 10-year homogenized series of GPS data. Q. J. R. Meteorolog. Soc. 140, 397–406. https://doi.org/10.1002/qj.2146.

Pacione, R., Araszkiewicz, A., Brockmann, E., Dousa, J., 2017. EPN-Repro2: A reference GNSS tropospheric data set over Europe. Atmos. Meas. Tech. 10, 1689–1705. https://doi.org/10.5194/amt-10-1689-2017.

Priego, J., Jones, J., Porres, M., Seco, A., 2016. Monitoring water vapour with GNSS during a heavy rainfall event in the Spanish Mediterranean area. Geomat. Nat. Haz. Risk 8, 1–13. https://doi.org/10.1080/19475705.2016.1201150.

REDIAM, R. de I.A. de la J. de A., 2014. Bioclimas de Andalucía. Un proyecto enmarcado en la elaboración de los Escenarios Locales de Cambio Climático de Andalucía actualizados al 5º Informe del IPCC.

Saastamoinen, J., 1972. Atmospheric correction for the troposphere and stratosphere in radio ranging satellites. In: The Use of Artificial Satellites for Geodesy. American Geophysical Union (AGU), pp. 247–251. https://doi.org/10.1029/GM015p0247.

Sguerso, D., Labbouz, L., Walpersdorf, A., 2015. 14 years of GPS tropospheric delays in the French-Italian border region: comparisons and first application in a case study. Appl. Geomat. 8, 1–13. https://doi.org/10.1007/s12518-015-0158-z.

Sousa, P.M., Trigo, R.M., Aizpurua, P., Nieto, R., Gimeno, L., Garcia-Herrera, R., 2011. Trends and extremes of drought indices throughout the 20th century in the Mediterranean. Nat. Hazards Earth Syst. Sci. 11, 33–51. https://doi.org/10.5194/nhess-11-33-2011.

Spinoni, J., Naumann, G., Vogt, J., Barbosa, P., 2015. European drought climatologies and trends based on a multi-indicator approach. Global Planet. Change 127, 50–57. https://doi.org/10.1016/j.gloplacha.2015.01.012.

Ssenyunzi, R.C., Oruru, B., D'ujanga, F.M., Realini, E., Barindelli, S., Tagliaferro, G., von Engeln, A., van de Giesen, N., 2020. Performance of ERA5 data in retrieving Precipitable Water Vapour over East African tropical region. Advances in Space Research 65, 1877–1893. https://doi.org/10.1016/j.asr.2020.02.003.

Ssenyunzi, R., Oruru, B., Mutonyi D'Ujanga, F., Realini, E., Barindelli, S., Tagliaferro, G., van de Giesen, N., 2019. Variability and accuracy of Zenith Total Delay over the East African Tropical Region. Adv. Space Res. 64. https://doi.org/10.1016/j.asr.2019.05.027.

Torres, B., Cachorro, V.E., Toledano, C., Ortiz de Galisteo, J.P., Berjón, A., de Frutos, A.M., Bennouna, Y., Laulainen, N., 2010. Precipitable water vapor characterization in the Gulf of Cadiz region (southwestern Spain) based on Sun photometer, GPS, and radiosonde data. J. Geophys. Res. Atmos. 115. https://doi.org/10.1029/2009JD012724.

Tramblay, Y., El Adlouni, S., Servat, E., 2013. Trends and variability in extreme precipitation indices over Maghreb countries. Nat. Hazards Earth Syst. Sci. 13, 3235–3248. https://doi.org/10.5194/nhess-13-3235-2013.

Vicente-Serrano, S.M., Beguería, S., López-Moreno, J.I., 2010. A multiscalar drought index sensitive to global warming: The standardized precipitation evapotranspiration index. J. Clim. 23, 1696–1718. https://doi.org/10.1175/2009JCLI2909.1.

Vicente-Serrano, S.M., Lopez-Moreno, J.-I., Beguería, S., Lorenzo-Lacruz, J., Sanchez-Lorenzo, A., García-Ruiz, J.M., Azorin-Molina, C., Morán-Tejeda, E., Revuelto, J., Trigo, R., Coelho, F., Espejo, F., 2014. Evidence of increasing drought severity caused by temperature rise in southern Europe. Environ. Res. Lett. 9, 044001. https://doi.org/10.1088/1748-9326/9/4/044001.

Vicente-Serrano, S.M., Tomas-Burguera, M., Beguería, S., Reig, F., Latorre, B., Peña-Gallardo, M., Luna, M.Y., Morata, A., González-Hidalgo, J.C., 2017. A high resolution dataset of drought indices for Spain. Data 2, 22. https://doi.org/10.3390/data2030022.

Wang, X., Zhang, K., Wu, S., Li, Z., Cheng, Y., Li, L., Yuan, H., 2018. The correlation between GNSS-derived precipitable water vapor and sea surface temperature and its responses to El Niño-Southern Oscillation. Remote Sens. Environ. 216, 1–12. https://doi.org/10.1016/j.rse.2018.06.029.

Yang, F., Guo, J., Meng, X., Shi, J., Xu, Y., Zhang, D., 2019. Determination of weighted mean temperature (Tm) lapse rate and assessment of its impact on Tm calculation. IEEE Access 7, 155028–155037. https://doi.org/10.1109/ACCESS.2019.2946916.

Zhang, Y., Cai, C., Chen, B., Dai, W., 2019. Consistency evaluation of precipitable water vapor derived from ERA5, ERA-interim, GNSS, and radiosondes over China. Radio Sci. 54, 561–571. https://doi.org/10.1029/2018RS006789.

Zhang, W., Zhang, H., Liang, H., Lou, Y., Cai, Y., Cao, Y., Zhou, Y., Liu, W., 2019. On the suitability of ERA5 in hourly GPS precipitable water vapor retrieval over China. J. Geod. 93, 1897–1909. https://doi.org/10.1007/s00190-019-01290-6.

Zhao, Q., Ma, X., Yao, W., Liu, Y., Du, Z., Yang, P., Yao, Y., 2019. Improved drought monitoring index using GNSS-derived precipitable water vapor over the loess plateau area. Sensors 19, 5566. https://doi.org/10.3390/s19245566.

Zhao, Q., Ma, X., Yao, W., Liu, Y., Yao, Y., 2020. A drought monitoring method based on precipitable water vapor and precipitation. J. Clim. 33, 10727–10741. https://doi.org/10.1175/JCLI-D-19-0971.1.

Zhao, Q., Liu, K., Li, Z., Liu, Y., Yao, Y., 2021. A novel ENSO monitoring index and its potential for drought application. J. Atmos. Sol. Terr. Phys. 225, 105762. https://doi.org/10.1016/j.jastp.2021.105762.

Zhao, Q., Zhang, X., Wu, K., Liu, Y., Li, Z., Shi, Y., 2022. Comprehensive precipitable water vapor retrieval and application platform based on various water vapor detection techniques. Remote Sens. (Basel) 14, 2507. https://doi.org/10.3390/rs14102507.

Please cite this article as: L. Retegui Schiettekatte, M. Selmira Garrido and M. Clara de Lacy, Use of GNSS and ERA5 precipitable water vapor based standardized precipitation conversion index for drought monitoring in the Mediterranean coast: A first case study in Southern Spain, Advances in Space Research, https://doi.org/10.1016/j.asr.2023.08.030